

## Conductance signatures of odd-frequency superconductivity in quantum spin Hall systems using a quantum point contact

C. Fleckenstein,<sup>\*</sup> N. Traverso Ziani, and B. Trauzettel*Institute of Theoretical Physics and Astrophysics, University of Würzburg, 97074 Würzburg, Germany*

(Received 28 February 2018; published 30 April 2018)

Topological superconductors give rise to unconventional superconductivity, which is mainly characterized by the symmetry of the superconducting pairing amplitude. However, since the symmetry of the superconducting pairing amplitude is not directly observable, its experimental identification is rather difficult. In our work, we propose a system, composed of a quantum point contact and proximity-induced  $s$ -wave superconductivity at the helical edge of a two-dimensional topological insulator, for which we demonstrate the presence of odd-frequency pairing and its intimate connection to unambiguous transport signatures. Notably, our proposal requires no time-reversal symmetry breaking terms. We discover the domination of crossed Andreev reflection over electron cotunneling in a wide range of parameter space, which is a quite unusual transport regime.

DOI: [10.1103/PhysRevB.97.134523](https://doi.org/10.1103/PhysRevB.97.134523)

### I. INTRODUCTION

Two-dimensional topological insulators (TIs), due to strong spin-orbit coupling, provide surface states with perfect spin-momentum locking [1–3]. Over the last decade of research, convincing evidence has been reported, proving the existence of those topological states in HgCdTe/HgTe [4,5] and InAs/GaSb quantum wells [6–10]. As long as electron-electron interactions are weak [11–14], the presence of time-reversal (TR) symmetry inevitably leads to a suppression of backscattering processes and thus provides dissipationless transport. This feature is usually attributed to superconductivity (SC). Interestingly, it is possible to combine both effects by proximity-induced  $s$ -wave superconductivity into the helical edge of a quantum spin Hall insulator (QSHI) [8,10,15–17]. There, the combination of conventional superconducting order and spin-momentum locking gives rise to unconventional superconductivity.

The associated order parameter is the superconducting pairing amplitude  $\mathcal{F}$ , which is directly related to the anomalous part of the retarded Green's function. According to the classification pioneered by Berezinskii [18], the pairing amplitude  $\mathcal{F}$  has to be totally antisymmetric under the exchange of all quantum numbers of the two constituent fermionic field operators. Having spin, orbit, and frequency as characteristics, this yields a set of four symmetry classes [19,20]. While conventional BCS superconductors are even in frequency, it has been shown that a special kind of unconventional superconductivity, that is odd in frequency, arises quite ubiquitously in spatially nonuniform systems in which spin rotation invariance is broken [20–24], such as SC-TI heterojunctions [25], or heterojunctions including additional ferromagnetic ordering [26–29]. However, since the symmetry of the pairing amplitude is not a quantum-mechanical observable, it is challenging to unambiguously probe odd-frequency pairing.

The first experimental signature attributed to odd-frequency SC has been identified as a long-range proximity effect in ferromagnetic Josephson junctions [30–32]. Subsequently, a paramagnetic Meißner effect has been proposed if odd-frequency SC is present [33–35]. Recently, it has furthermore been demonstrated that odd-frequency SC can be directly assigned to particular transport properties, using a QSHI in proximity to both  $s$ -wave SC and ferromagnetic ordering [28,36]. At the helical edge, the ferromagnetic ordering allows for odd-frequency equal-spin pairing, intimately related to crossed Andreev reflection (CAR), where an incident electron is transmitted through the scattering region as a hole and scattered into a second, spatially separated lead [37–41]. Spin-momentum locking then implies the equivalence of this transport channel with the creation of an equal-spin triplet Cooper pair in the heterostructure [42,43]. Using resonances between hybridizing Majorana bound states, it has been proposed that CAR can overcome electron cotunneling (EC) across the junction, and thus yields a smoking-gun evidence of odd-frequency SC. However, despite interesting applications [44–48], it is experimentally challenging to induce ferromagnetic ordering in two-dimensional (2D) TIs and more feasible setups are needed, in which TR symmetry is preserved.

In this paper, we present a simple system, composed of proximity-induced  $s$ -wave pairing and a quantum point contact (QPC) at the helical edge of a 2D TI (see Fig. 1). This setup has recently been investigated with an emphasis on Kramers pairs of Majorana fermions, present when a superconducting phase shift of  $\pi$  is applied between separate superconductors, covering the two edges [49]. For our purposes, this setup has the crucial advantage that no ferromagnets are involved, but it still contains the desired feature: odd-frequency equal-spin pairing with direct connection to the differential conductance of the system. More specifically, we demonstrate that such a QPC can generate equal-spin triplet pairing if axial spin symmetry is broken. Locally, equal-spin correlations are suppressed. However, nonlocal correlations appear across the QPC/junction. They inevitably lead to nonvanishing CAR between contacts 1

<sup>\*</sup>christoph.fleckenstein@physik.uni-wuerzburg.de

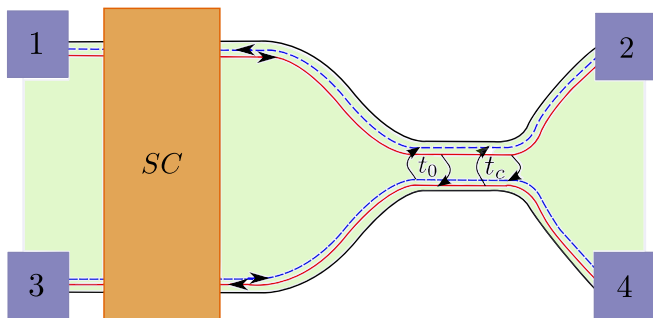


FIG. 1. Schematic of the system: Each edge of a quantum spin Hall sample is coupled to separate contacts 1–4. The sample itself contains a heterostructure, composed of a region with proximity-induced  $s$ -wave superconductivity and a quantum point contact including the terms  $t_0$  and  $t_c$ , defined in Eqs. (4) and (5).

and 2 in Fig. 1. Additionally, the QPC provides three accessible channels for EC. Therefore, the EC per channel is reduced. The combination of both effects leads to a domination of CAR over EC for a wide range in parameter space. This dominance is observable in the linear (nonlocal) conductance, as it directly probes the difference between CAR and EC, which hence implies the presence of odd-frequency SC.

The article is structured as follows: In Sec. II, we introduce the model and give a theoretical description of the symmetry of the superconducting pairing amplitude in terms of the corresponding Green's function. In Sec. III, we analyze the different pairing amplitudes present in our system, while in Sec. IV we discuss their relation to transport channels by means of the differential (nonlocal) conductance. Finally, we conclude in Sec. V. Technical details are provided in two Appendices.

## II. MODEL AND GREEN'S FUNCTION

### A. Model

The system we investigate is formed by the helical edge of a 2D TI, partially covered by an  $s$ -wave superconductor and coupled to a QPC, as schematically shown in Fig. 1. The physics of each edge of the 2D TI channel is captured by the effective edge state Hamiltonian

$$H_{\lambda,0} = \int dx \Psi_{\lambda}^{\dagger}(x) \mathcal{H}_{\lambda}(x) \Psi_{\lambda}(x) \quad (1)$$

with Hamiltonian density

$$\mathcal{H}_{\lambda}(x) = -\lambda \hbar v_F i \partial_x \tau_z \sigma_z - \mu(x) \tau_z \sigma_0 + \Delta(x) \tau_x \sigma_0 \quad (2)$$

and basis

$$\Psi_{\lambda}(x) = (\psi_{\lambda,\uparrow}(x), \psi_{\lambda,\downarrow}(x), \psi_{\lambda,\downarrow}^{\dagger}(x), -\psi_{\lambda,\uparrow}^{\dagger}(x))^T, \quad (3)$$

where  $\lambda \in \{+, -\}$  (for upper and lower edge). The Pauli matrices  $\tau_i, \sigma_i$  with  $i \in \{x, y, z\}$  act on particle-hole and spin space, respectively. We assume a spatially varying chemical potential  $\mu(x)$ . Furthermore, we include a proximity-induced  $s$ -wave pairing by  $\Delta(x)$  with the characteristic length scale  $\xi_{\Delta} = \hbar v_F / \Delta$ . In the following we fix  $\hbar v_F = 1$ . In the constriction of the quantum point contact, we additionally add two TR invariant scattering processes across the edges [49–53], which

are (i) spin-conserving backscattering

$$H_{t_0} = \int dx t_0(x) [\psi_{+,\uparrow}^{\dagger}(x) \psi_{-,\uparrow}(x) + \psi_{+,\downarrow}^{\dagger}(x) \psi_{-,\downarrow}(x)] + \text{H.c.}, \quad (4)$$

and (ii) forward scattering, breaking axial spin symmetry [11,54–58]

$$H_{t_c} = \int dx t_c(x) [\psi_{+,\uparrow}^{\dagger}(x) \psi_{-,\downarrow}(x) - \psi_{+,\downarrow}^{\dagger}(x) \psi_{-,\uparrow}(x)] + \text{H.c.} \quad (5)$$

The full Hamiltonian of the system then reads

$$H = \sum_{\lambda} H_{\lambda,0} + H_{t_0} + H_{t_c}. \quad (6)$$

In compact form, we can state the full Hamiltonian density as

$$\mathcal{H}(x) = -i \partial_x s_z \tau_z \sigma_z - \mu(x) s_0 \tau_z \sigma_0 + \Delta(x) s_0 \tau_x \sigma_0 + t_0(x) s_x \tau_z \sigma_0 - t_c(x) s_y \tau_z \sigma_y \quad (7)$$

using the basis  $\Phi(x) = (\Psi_+(x), \Psi_-(x))^T$  and the Pauli matrices  $s_i$  with  $i \in \{x, y, z\}$  acting on edge space. We model the heterostructure shown in Fig. 1 by using piecewise constant potentials  $\Delta(x) = \Delta \theta(x) \theta(l_s - x)$ ,  $t_0(x) = t_0 \theta(x - x_q) \theta(x_q + l_q - x)$ , and  $t_c(x) = t_c \theta(x - x_q) \theta(x_q + l_q - x)$  with  $\theta(x)$  the Heaviside function. Here,  $\Delta$ ,  $t_0$ , and  $t_c$  are real and positive parameters, while  $x_q$  marks the beginning of the quantum point contact. Furthermore,  $l_q$  and  $l_s$  are the length of the constriction and the superconductor, respectively.

We can solve the first-order differential Schrödinger equation  $\mathcal{H}(x)\Phi(x) = \omega\Phi(x)$  by integration. From

$$\partial_x \Phi(x) = i[h(x) + s_z \tau_z \sigma_z \omega] \Phi(x) \quad (8)$$

with

$$h(x) = s_z \tau_z \sigma_z [\mu(x) s_0 \tau_z \sigma_0 - \Delta(x) s_0 \tau_x \sigma_0 - t_0(x) s_x \tau_z \sigma_0 + t_c(x) s_y \tau_z \sigma_y], \quad (9)$$

we find the general solution

$$\Phi(x) = \mathcal{S}_{\leftarrow} U(x, x_0) \Phi_0(x_0), \quad (10)$$

where

$$U(x, x_0) = \exp \left\{ i \int_{x_0}^x dx [h(x) + s_z \tau_z \sigma_z \omega] \right\}. \quad (11)$$

In Eq. (10),  $\mathcal{S}_{\leftarrow}$  is a spatial-ordering operator, required to order all operators, acting on  $\Phi_0(x_0)$ , with their spatial coordinates increasing from right to left [59]. As we only apply piecewise constant potentials, we can neglect  $\mathcal{S}_{\leftarrow}$  whenever the integration runs within a homogeneous section. Together with the condition of continuity of the wave function at each interface between sections of different potentials, the scattering problem, defined by the Hamiltonian (7), can be formulated as

$$\Phi_{\text{out},l}(x_q + l_q) = U_l(x_q + l_q, x_q) U_0(x_q, l_s) U_{sc}(l_s, 0) \Phi_{\text{in},l}(0) \quad (12)$$

with the propagators  $U_l(x_l, x'_l)$ ,  $U_0(x_0, x'_0)$ , and  $U_{sc}(x_{sc}, x'_{sc})$  defined according to Eq. (11) in the bounds  $\{x_l, x'_l\} \in [x_q, x_q + l_q]$ ,  $\{x_0, x'_0\} \in [l_s, x_q]$ , and  $\{x_{sc}, x'_{sc}\} \in [0, l_s]$ . The form of the

vectors  $\Phi_{\text{in},l}(x)$  and  $\Phi_{\text{out},l}(x)$  are fixed by spin-momentum locking, together with the basis of Eq. (3).

However, we still need to select a channel for an incident particle, whose amplitude we fix to unity [60]. This procedure allows us to derive eight independent scattering states denoted by the index  $l \in [1, 8]$ . They are classified according to the incoming amplitude: incoming electron/hole from the right/left in edge  $+/-$ . A detailed derivation thereof is provided in Appendix A. Consequently, an incoming particle  $\chi \in \{e, h\}$  from edge  $\lambda$  can be reflected as an electron with amplitude  $r_{\chi e}^{\lambda\lambda'}(\omega)$  or as a hole with amplitude  $r_{\chi h}^{\lambda\lambda'}(\omega)$  into edge  $\lambda'$ . Likewise, transmission is possible with amplitude  $t_{\chi e}^{\lambda\lambda'}(\omega)$  and  $t_{\chi h}^{\lambda\lambda'}(\omega)$ .

### B. Scattering state Green's function

From the scattering states, it is possible to construct the Green's function of the system [61,62]. With the equation of motion, it can be demonstrated in general, that for any time-independent Hamiltonian and any  $x \neq x'$ , any Green's function

$$\hat{G}^{R/A}(x, x', \omega) = \int dt e^{i(\omega \pm i0^+)t} \hat{G}^{R/A}(x, x', t) \quad (13)$$

with  $\hat{G}^R(x, x', t) = -i\theta(t)\{\Psi(x, t), \Psi^\dagger(x', 0)\}$  and  $\hat{G}^A(x, x', t) = \hat{G}^R(x', x, -t)^\dagger$ , can be constructed from eigenstates  $\Phi(x, \omega)$  of the Hamiltonian  $\mathcal{H}(x, \hat{p}_x)$  and eigenstates  $\tilde{\Phi}(x', \omega)$  of its transposed  $\mathcal{H}^T(x', -\hat{p}_{x'})$ , i.e.,

$$\hat{G}_{n,m}^{R/A}(x, x', \omega) = \sum_{i,j} a_{i,j}^{R/A}(\omega) \phi_{i,n}(x, \omega) \tilde{\phi}_{j,m}(x', \omega), \quad (14)$$

where  $\phi_{i,n}$  and  $\tilde{\phi}_{j,m}$  are the  $n$ th and  $m$ th, components of the  $i$ th and  $j$ th eigenstates. The indices  $i, j$  then run over all independent scattering states. Likewise, by integration of the equation  $[\omega - \mathcal{H}(x, \hat{p}_x)]\hat{G}^{R/A}(x, x', \omega) = \delta(x - x')$ ,  $\hat{G}^{R/A}(x, x', \omega)$  has to satisfy a discontinuity at  $x = x'$ ,

$$\lim_{\epsilon \rightarrow 0} [\hat{G}^{R/A}(x' + \epsilon, x', \omega) - \hat{G}^{R/A}(x' - \epsilon, x', \omega)] = C. \quad (15)$$

For the Hamiltonian, given in Eq. (7),  $C = is_z \tau_z \sigma_z$ . Any function of the form of Eq. (14), together with the constraint (15), provides a valid Green's function. However, for deriving a particular one, such as retarded or advanced, more information is needed to determine the coefficients  $a_{i,j}^{R/A}(\omega)$ . As all  $a_{i,j}^{R/A}(\omega)$  are independent of  $x$  and  $x'$ , it is sufficient to know the exact form of the Green's function of interest in a single set of points  $x_0$  and  $x'_0$ . Since it is significantly easier to calculate the Green's function in a semi-infinite domain, it is suitable to position  $x_0$  and  $x'_0$  far in the left or right reservoirs.

We are interested in the superconducting pairing amplitude, which is related to the anomalous part of the retarded Green's function. To compute the retarded Green's function in the semi-infinite lead, we apply *outgoing wave boundary conditions* [63,64]. We split the Green's function into two parts  $\hat{G}^R(x, x', \omega) = \hat{G}_{<}^R(x, x', \omega)\theta(x' - x) + \hat{G}_{>}^R(x, x', \omega)\theta(x - x')$ . We explicitly derive the retarded Green's function in the leftmost lead ( $x_0, x'_0 < 0$ ) in

Appendix B. Then, we can construct the Green's function of any  $x$  and  $x'$  as

$$\hat{G}^R(x, x', \omega) = U(x, x_0) \hat{G}^R(x_0, x'_0, \omega) \tilde{U}^T(x', x'_0), \quad (16)$$

where  $\tilde{U}(x', x'_0)$  is the corresponding propagator derived from  $\mathcal{H}^T(x', -\hat{p}_{x'})$ . For our system, the Green's function is an  $8 \times 8$  matrix with the general structure

$$\hat{G}^R(x, x', \omega) = \begin{pmatrix} \hat{G}_{++}^R(x, x', \omega) & \hat{G}_{-+}^R(x, x', \omega) \\ \hat{G}_{+-}^R(x, x', \omega) & \hat{G}_{--}^R(x, x', \omega) \end{pmatrix}. \quad (17)$$

Each  $\hat{G}_{\lambda\lambda'}^R(x, x', \omega)$  is itself a  $4 \times 4$  matrix, representing the intraedge Green's function for  $\lambda = \lambda'$  and the interedge Green's function for  $\lambda = -\lambda'$ , respectively. Furthermore, each  $\hat{G}_{\lambda\lambda'}^R(x, x', \omega)$  can be decomposed into

$$\hat{G}_{\lambda\lambda'}^R(x, x', \omega) = \begin{pmatrix} \hat{G}_{\lambda\lambda', ee}^R(x, x', \omega) & \hat{G}_{\lambda\lambda', eh}^R(x, x', \omega) \\ \hat{G}_{\lambda\lambda', he}^R(x, x', \omega) & \hat{G}_{\lambda\lambda', hh}^R(x, x', \omega) \end{pmatrix}. \quad (18)$$

The off-diagonal parts of  $\hat{G}_{\lambda\lambda'}^R(x, x', \omega)$  thereby carry the information about the superconducting pairing. In the basis of Eq. (3), we can directly illustrate the spin texture of the pairing with the decomposition into Pauli matrices

$$\hat{G}_{\lambda\lambda', eh}^R(x, x', \omega) = f_{\lambda\lambda', 0}^R(x, x', \omega) \sigma_0 + f_{\lambda\lambda', j}^R(x, x', \omega) \sigma_j, \quad (19)$$

where  $j \in \{x, y, z\}$ . In Eq. (19),  $f_{\lambda\lambda', 0}^R(x, x', \omega)$  is the singlet ( $S$ ) component of the pairing, relating to the antisymmetric spin configuration ( $\uparrow\downarrow - \downarrow\uparrow$ ). Likewise, the triplet ( $T$ ) components relate to the symmetric spin configuration with  $f_{\lambda\lambda', z}^R(x, x', \omega)$  with ( $\uparrow\downarrow + \downarrow\uparrow$ ), and the equal-spin pairing  $f_{\lambda\lambda', \uparrow\uparrow}^R = f_{\lambda\lambda', x}^R(x, x', \omega) - if_{\lambda\lambda', y}^R(x, x', \omega)$ ,  $f_{\lambda\lambda', \downarrow\downarrow}^R = f_{\lambda\lambda', x}^R(x, x', \omega) + if_{\lambda\lambda', y}^R(x, x', \omega)$ , having  $\uparrow\uparrow, \downarrow\downarrow$  configuration, respectively. From the definition of the advanced Green's function  $\hat{G}^A(x, x', \omega) = \hat{G}^R(x', x, \omega)^\dagger$ , using Eq. (13), we can translate the antisymmetry of the pairing amplitudes under exchange of the constituents into relations between retarded and advanced pairing amplitudes

$$f_{\lambda\lambda', 0}^R(x, x', \omega) = f_{\lambda\lambda', 0}^A(x', x, -\omega), \quad (20)$$

$$f_{\lambda\lambda', j}^R(x, x', \omega) = -f_{\lambda\lambda', j}^A(x', x, -\omega) \quad (21)$$

with  $j \in \{x, y, z\}$ . Here,  $f_{\lambda\lambda', l}^A(x', x, \omega)$  ( $l \in \{0, x, y, z\}$ ) is built from the advanced Green's function. Besides spin, orbit, and frequency, in case  $\lambda \neq \lambda'$ , we additionally have the edge index as degree of freedom to fulfill Eqs. (20) and (21) [65]. However, in this paper, we will focus on the symmetry classification for one edge, i.e.,  $\lambda = \lambda'$ .

We can further decompose the symmetry requirements of Eqs. (20) and (21) into orbital and frequency symmetries. The orbital symmetries are captured by

$$f_{\lambda\lambda', l}^R(x, x', \omega) = \zeta_{\lambda\lambda', l}^{R,+}(x, x', \omega) + \zeta_{\lambda\lambda', l}^{R,-}(x, x', \omega) \quad (22)$$

with even ( $E$ ) and odd ( $O$ ) parts  $\zeta_{\lambda\lambda', l}^{R,\pm}(x, x', \omega) = 1/2[f_{\lambda\lambda', l}^R(x, x', \omega) \pm f_{\lambda\lambda', l}^R(x', x, \omega)]$ . To obey Eqs. (20) and (21), the symmetries in  $\omega$  are then required to be

$$\zeta_{\lambda\lambda', 0}^{R,\pm}(x, x', \omega) = \pm \zeta_{\lambda\lambda', 0}^{A,\pm}(x, x', -\omega), \quad (23)$$

$$\zeta_{\lambda\lambda', j}^{R,\pm}(x, x', \omega) = \mp \zeta_{\lambda\lambda', j}^{A,\pm}(x, x', -\omega), \quad (24)$$

where  $j \in \{x, y, z\}$  and  $\zeta_{\lambda\lambda,j}^{A,\pm}(x, x', -\omega), \zeta_{\lambda\lambda,0}^{A,\pm}(x, x', -\omega)$  are the even and odd orbital parts of the advanced pairing amplitude. Equations (20)–(24) describe all possible symmetry classes, which are coined in the order frequency, spin, and orbit as ESE [ $\zeta_{\lambda\lambda,0}^{R,+}(x, x', \omega)$ ], OSO [ $\zeta_{\lambda\lambda,0}^{R,-}(x, x', \omega)$ ], ETO [ $\zeta_{\lambda\lambda,j}^{R,-}(x, x', \omega)$ ], and OTE [ $\zeta_{\lambda\lambda,j}^{R,+}(x, x', \omega)$ ].

### III. LOCAL AND NONLOCAL PAIRING SYMMETRIES

As translation symmetry is broken in heterostructures, it is inevitable that any pairing is constituted by a mixture of even and odd orbital parts. Furthermore, since spin-momentum locking naturally implies triplet pairing, by construction ETO and OTE pairings are expected. In bare TI-SC heterojunctions, triplet pairing exists only in the form of the amplitude  $f_{\lambda\lambda,z}^R(x, x', \omega)$  corresponding to the spin configuration ( $\uparrow\downarrow + \downarrow\uparrow$ ). It is thus difficult to discriminate this triplet amplitude in any (spin sensitive) conductance measurement from their singlet counterparts. This dilemma can be overcome if equal-spin pairing is generated in the heterojunction. Then, the CAR process across the junction, which is usually suppressed by spin-momentum locking [66], is directly related to the injection of a Cooper pair with  $\uparrow\uparrow$  ( $\downarrow\downarrow$ ) spin texture. A way to design  $\uparrow\uparrow$  or  $\downarrow\downarrow$  pairing at the helical edge is to include ferromagnetic ordering [28]. As it seems to be very difficult to combine ferromagnetic insulators and TIs in the laboratory, we identify a setup, in the absence of ferromagnetic ordering, in which (odd-frequency)  $\uparrow\uparrow$  and  $\downarrow\downarrow$  pairing at the helical edge can be generated. This is possible, due to the simultaneous presence of two TR invariant coupling terms [see Eqs. (4) and (5) above]. By introducing a spin preserving coupling between the edges, Eq. (4) generates Andreev bound states between SC and QPC that extend over both edges. Additionally, Eq. (5) breaks axial spin symmetry and thus allows for  $\uparrow\uparrow$  and  $\downarrow\downarrow$  pairing in each edge.

To demonstrate this effect, we proceed with the calculation of the pairing amplitudes. We apply Eq. (16), with  $G^R(x_0, x'_0, \omega)$  for  $x_0, x'_0 \rightarrow 0^-$  and calculate the amplitudes  $f_{++j}^R(x, x, \omega)$  with  $j \in \{0, z\}$  and  $x \in [0, x_q + l_q]$ . As  $x = x'$ , we naturally compute the ESE and OTE symmetries by construction. We find that local equal-spin correlations are totally suppressed throughout the whole junction  $f_{++\uparrow}^R(x, x, \omega) = 0$ . However, nonlocal equal-spin correlations are present in the form of  $f_{++\uparrow}^R(x, x + \xi, \omega)$  with  $x \in [0, x_q + l_q - \xi]$ . The results are depicted in Fig. 2.

The suppression of local equal-spin pairing amplitudes is different with respect to the TR symmetry breaking case, where it is typically related to the amplitude of electron-electron (hole-hole) reflection  $r_{ee}^{++}(\omega)$  [ $r_{hh}^{++}(\omega)$ ], which vanish by TR symmetry in our system. The nonlocal equal-spin pairing  $f_{++\uparrow}^R(x, x + \xi, \omega)$  created by the QPC, however, is finite whenever there is at least one point  $\chi$  with  $\chi \in [x, x + \xi]$  that belongs to the region of the QPC. This is realized when at least one of the two spatial coordinates of the corresponding correlation function is part of the QPC region, i.e.,  $x, x + \xi \in [x_q, x_q + l_q]$  [see Figs. 2(c) and 2(d)], or when the pairing happens across the whole QPC/junction (Fig. 3). In both cases, even- and odd-frequency parts appear [Figs. 2(c) and 2(d)]. As expected, the nonlocal pairing  $f_{++\uparrow}^R(0, x_q + l_q, \omega)$  has a

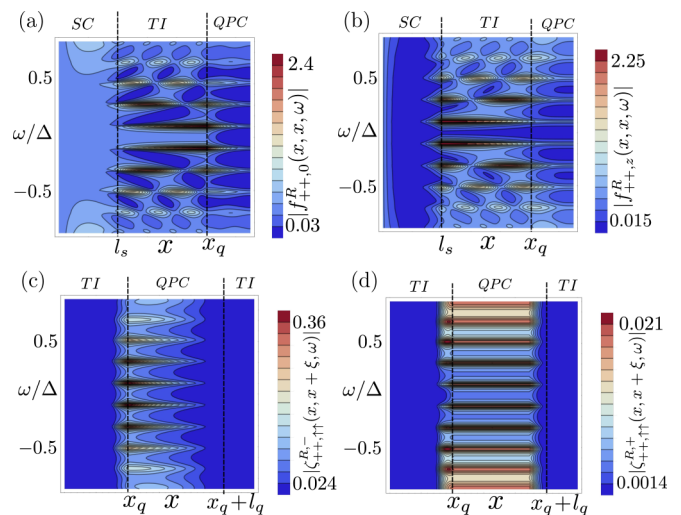


FIG. 2. Superconducting pairing in the heterojunction of Fig. 1 as a function of position  $x$  and energy  $\omega$ . (a) and (b) illustrate the local singlet and triplet ( $\uparrow\downarrow + \downarrow\uparrow$ ) pairing, while (c) and (d) show the even- and odd-frequency equal-spin pairing with  $x' = x + \xi$  and  $\xi = 0.5\xi_\Delta$ . We use the parameters  $\mu = 0, t_0/\Delta = t_c/\Delta = t/\Delta = 0.4, l_s = 4\xi_\Delta, l_q = 3\xi_\Delta$ , and  $x_q = 10\xi_\Delta$ .

maximum, whenever the energy of an Andreev bound state is matched (see Fig. 3). Using Eqs. (22) and (23), we derive that the non-local equal-spin pairing across the junction is equally distributed from OTE and ETO parts. This turns out to be a very generic result, implied by spin-momentum locking. As the retarded Green's function implements time-ordering, nonlocal equal-spin pairing from  $x = 0$  to  $x' = x_q + l_q$  represents a correlation acting, for instance, forward in time and forward in space, while correlations from  $x = x_q + l_q$  to  $x' = 0$  describe the corresponding process backward in space. For a defined pairing amplitude [ $f_{\lambda\lambda,\uparrow\uparrow}^R(0, x_q + l_q, \omega)$  or  $f_{\lambda\lambda,\downarrow\downarrow}^R(0, x_q + l_q, \omega)$ ] at the helical edge, only one of the two processes is finite due to spin-momentum locking. This behavior inverts as  $x$  and  $x'$  are exchanged. Consequently, from Eq. (22), we conclude that ETO and OTE pairing amplitudes are necessarily equal. Importantly, the presence of both coupling terms of Eqs. (4) and (5) is crucial for finite equal-spin pairing at a single edge (Fig. 4).

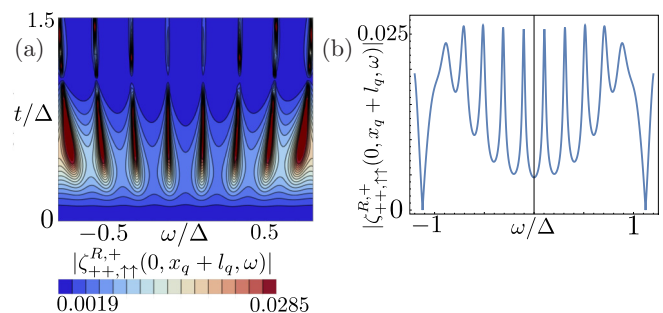


FIG. 3. (a) OTE part of the pairing amplitude  $|f_{++\uparrow}^R(0, x_q + l_q, \omega)|$  as a function of coupling strength  $t/\Delta = t_0/\Delta = t_c/\Delta$  and energy  $\omega/\Delta$ . (b) Line cut from (a) for  $t/\Delta = t_0/\Delta = t_c/\Delta = 0.4$  and the other parameters given in Fig. 2.



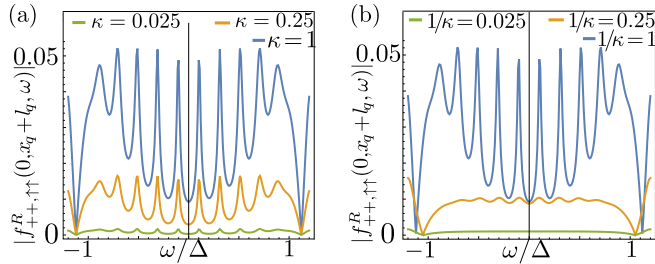


FIG. 4. Nonlocal  $\uparrow\uparrow$  pairing as a function of  $\omega$  for different values of the QPC coupling. We introduce the dimensionless parameter ratio  $\kappa = t_c/t_0$ . Other parameters are the same as in Fig. 2.

#### IV. TRANSPORT SIGNATURES

As a consequence of spin-momentum locking in our structure, the observable directly related to the nonlocal equal-spin pairing is the CAR process. However, an incident particle, while transmitted, can either undergo CAR or EC. Since the two processes carry opposite charge, they enter with different signs in the nonlocal conductance. For concreteness, we are interested in the nonlocal differential conductance  $G_{21}(\omega)$ , measuring the transmission between contacts 1 and 2 of Fig. 1 at excitation energy  $\omega$ . By definition  $G_{21}(\omega)$  is given as the differential change of the current at contact 2, when a voltage  $V_1$  is applied at contact 1, i.e.,

$$G_{21}(eV_1) = -\frac{\partial I_2(eV_1)}{\partial V_1} = \frac{e^2}{h} [ |t_{eh}^{++}(eV_1)|^2 - |t_{ee}^{++}(eV_1)|^2 ]. \quad (25)$$

The coefficients  $t_{eh}^{++}(\omega)$  and  $t_{ee}^{++}(\omega)$  are obtained from the corresponding scattering problem, defined in Appendix A. Clear evidence of CAR is thus only provided if  $G_{21}(eV_1) > 0$ . Unfortunately, this is not the generic case [39,67], especially not at the helical edge, where CAR is additionally assigned to a spin configuration of the attributed Cooper pair [28]. Our system, however, has two major advantages in this respect: First, it provides nonlocal odd-frequency equal-spin pairing across the junction, directly related to  $t_{eh}^{++}(\omega)$ , without any TR breaking term. Second, as the QPC includes the other edge and we break axial spin symmetry, there are now three open channels available for EC. This possibility yields a reduced rate  $t_{ee}^{\lambda\lambda'}(\omega)$  for each individual channel. The combination of those two effects leads to a domination of CAR over EC in a large domain of parameter space, which hence obeys a nonlocal conductance  $G_{21}(\omega) > 0$  (see Fig. 5). Notably, unlike other proposals, ours implies that nearly no fine-tuning is needed in order to measure CAR. Comparing Figs. 3 and 5(a), we notice that the area of positive nonlocal conductance is indeed related to the area of pronounced nonlocal equal-spin pairing, where in both cases we recognize the presence of Andreev bound states in the form of maxima.

##### Influence of the chemical potential

When including a finite chemical potential  $\mu$  in the heterojunction, we obtain an asymmetry of the nonlocal conductance signature  $G_{21}(\omega)$  with respect to  $\omega \rightarrow -\omega$  [see Figs. 6(c) and 6(d)]. For positive chemical potential, negative excitation ener-

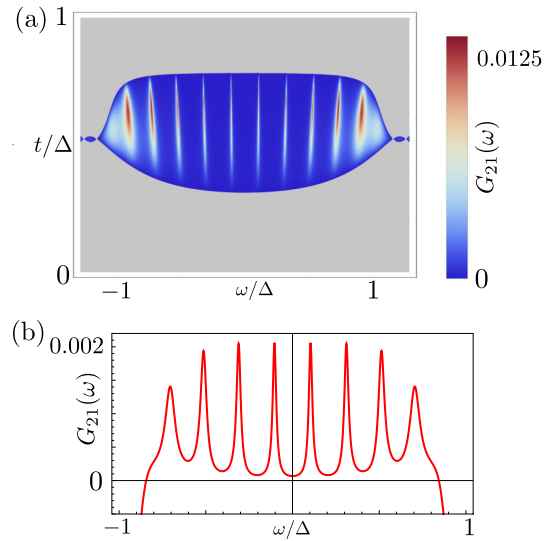


FIG. 5. (a) Nonlocal conductance  $G_{21}(\omega)$  in units of  $e^2/h$  for the setup shown in Fig. 1 with the parameters of Fig. 2. In the gray area we obtain  $G_{21}(\omega) < 0$ , while in the colored region we have  $G_{21}(\omega) > 0$ . (b) Line cut for  $t/\Delta = 0.4$ .

gies are favored in showing a nonlocal conductance  $G_{21}(\omega) > 0$  and vice versa. The explanation for this effect is found in the dispersion relation of the (infinitely extended) QPC [see Figs. 6(a) and 6(b)]. While the forward scattering  $H_{t_c}$  is not affected by  $\mu$ , the backscattering term  $H_{t_0}$  is sensitive to the chemical potential, which acts in the opposite way to electron- and holelike excitations. For  $\mu \neq 0$  we can thus emphasize or suppress backscattering on electron- and holelike states by

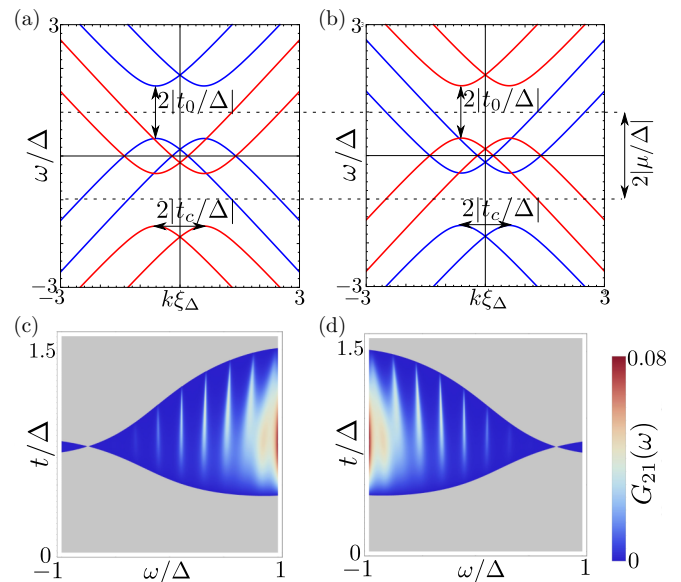


FIG. 6. (a), (b) Dispersion relation of the QPC with the parameters  $t_0/\Delta = t_c/\Delta = 0.6$ , and  $\mu/\Delta = -1$  in (a) and  $\mu/\Delta = 1$  in (b). Electronlike excitations are shown in blue, and holelike excitations in red. (c), (d) Nonlocal conductance  $G_{21}(\omega)$  in units of  $e^2/h$  for the parameters  $l_s = 3\xi_\Delta$ ,  $l_q = 2\xi_\Delta$ ,  $x_q = 9\xi_\Delta$ , and  $\mu/\Delta = -1$  in (c), and  $\mu/\Delta = 1$  in (d), respectively.

finite excitation energies  $\omega \neq 0$ . To obtain  $G_{21}(\omega) > 0$  it is important to enhance the transmission of holelike excitations and likewise suppress transmission of electronlike excitations across the QPC. Hence, comparing with Figs. 6(a) and 6(b), for positive chemical potential, negative excitation energies are favorable and vice versa. This is indeed consistent with our results [see Figs. 6(c) and 6(d)].

## V. CONCLUSION

In this paper, we have demonstrated the emergence of equal-spin triplet superconductivity at the helical edge without the need of ferromagnetic ordering. This can be achieved by the combination of proximity-induced  $s$ -wave pairing and scattering off a QPC. In the absence of axial spin symmetry, the QPC provides two possible coupling terms. In the presence of both, equal-spin triplet pairing is generated. While its local pairing amplitude is suppressed throughout the junction, nonlocal correlations arise whenever the spatial coordinates of the correlation function (partially) include the QPC or extend across it. On the basis of a symmetry analysis, we verify the (partial) odd-frequency nature of the nonlocal equal-spin pairing amplitude. This correlation is intimately related to the creation of equal-spin triplet Cooper pairs in the junction and thus to the process of cCAR. Notably, the QPC provides us with direct access to this transmission channel, as it likewise lowers the rate of EC. Thus, the nonlocal conductance  $G_{21}(\omega)$ , given by the difference between CAR and EC, exhibits a positive signal. The domination of CAR over EC is given for a wide range in parameter space and thus persists without fine-tuning. The presence of CAR provides unambiguous evidence of odd-frequency superconductivity at the helical edge.

## ACKNOWLEDGMENTS

We thank Felix Keidel for interesting discussions. We acknowledge financial support by the DFG (SPP1666 and SFB1170 ‘‘ToCoTronics’’), the Helmholtz Foundation (VITI), the ENB Graduate school on ‘‘Topological Insulators,’’ and the Studienstiftung des Deutschen Volkes.

## APPENDIX A: SCATTERING PROBLEM

The scattering problem, defined by Eq. (12), has eight independent solutions, classified according to the incident particle. Four of them,  $\Phi_{\text{in},1-4}(x)$ , represent a particle incident from the left. At  $x = 0$  we have

$$\Phi_{\text{in},1}(0) = (1, r_{ee}^{++}, r_{eh}^{++}, 0, r_{ee}^{+-}, 0, 0, r_{eh}^{+-})^T, \quad (\text{A1})$$

$$\Phi_{\text{in},2}(0) = (0, r_{he}^{++}, r_{hh}^{++}, 1, r_{he}^{+-}, 0, 0, r_{hh}^{+-})^T, \quad (\text{A2})$$

$$\Phi_{\text{in},3}(0) = (0, r_{ee}^{-+}, r_{eh}^{-+}, 0, r_{ee}^{--}, 1, 0, r_{eh}^{--})^T, \quad (\text{A3})$$

$$\Phi_{\text{in},4}(0) = (0, r_{he}^{-+}, r_{hh}^{-+}, 0, r_{he}^{--}, 0, 1, r_{hh}^{--})^T. \quad (\text{A4})$$

At  $x = x_q + l_q$ , the corresponding outgoing modes are

$$\Phi_{\text{out},1}(x_q + l_q) = (t_{ee}^{++}, 0, 0, t_{eh}^{++}, 0, t_{ee}^{+-}, t_{eh}^{+-}, 0)^T, \quad (\text{A5})$$

$$\Phi_{\text{out},2}(x_q + l_q) = (t_{he}^{++}, 0, 0, t_{hh}^{++}, 0, t_{he}^{+-}, t_{hh}^{+-}, 0)^T, \quad (\text{A6})$$

$$\Phi_{\text{out},3}(x_q + l_q) = (t_{ee}^{-+}, 0, 0, t_{eh}^{-+}, 0, t_{ee}^{--}, t_{eh}^{--}, 0)^T, \quad (\text{A7})$$

$$\Phi_{\text{out},4}(x_q + l_q) = (t_{he}^{-+}, 0, 0, t_{hh}^{-+}, 0, t_{he}^{--}, t_{hh}^{--}, 0)^T. \quad (\text{A8})$$

All scattering amplitudes are functions of the excitation energy  $\omega$ , where the explicit dependence is dropped here for simplicity. Furthermore, each transmission amplitude has to be multiplied by a phase factor containing the position, energy, and chemical potential. However, since all transport properties do not depend on phases of the transmission amplitudes and as they do not enter into the lead Green’s function, derived below, we absorb these phases in the amplitudes.

Another set of four independent scattering states is constituted from a particle incident from the right  $\Phi_{\text{out},5-8}(x)$ :

$$\Phi_{\text{out},5}(x_q + l_q) = (\rho_{ee}^{++}, 1, 0, \rho_{eh}^{++}, 0, \rho_{ee}^{+-}, \rho_{eh}^{+-}, 0)^T, \quad (\text{A9})$$

$$\Phi_{\text{out},6}(x_q + l_q) = (\rho_{he}^{++}, 0, 1, \rho_{hh}^{++}, 0, \rho_{he}^{+-}, \rho_{hh}^{+-}, 0)^T, \quad (\text{A10})$$

$$\Phi_{\text{out},7}(x_q + l_q) = (\rho_{ee}^{-+}, 0, 0, \rho_{eh}^{-+}, 1, \rho_{ee}^{--}, \rho_{eh}^{--}, 0)^T, \quad (\text{A11})$$

$$\Phi_{\text{out},8}(x_q + l_q) = (\rho_{he}^{-+}, 0, 0, \rho_{hh}^{-+}, 0, \rho_{he}^{--}, \rho_{hh}^{--}, 1)^T, \quad (\text{A12})$$

partially transmitted to the left:

$$\Phi_{\text{in},5}(0) = (0, \tau_{ee}^{++}, \tau_{eh}^{++}, 0, \tau_{ee}^{+-}, 0, 0, \tau_{eh}^{+-})^T, \quad (\text{A13})$$

$$\Phi_{\text{in},6}(0) = (0, \tau_{he}^{++}, \tau_{hh}^{++}, 0, \tau_{he}^{+-}, 0, 0, \tau_{hh}^{+-})^T, \quad (\text{A14})$$

$$\Phi_{\text{in},7}(0) = (0, \tau_{ee}^{-+}, \tau_{eh}^{-+}, 0, \tau_{ee}^{--}, 0, 0, \tau_{eh}^{--})^T, \quad (\text{A15})$$

$$\Phi_{\text{in},8}(0) = (0, \tau_{he}^{-+}, \tau_{hh}^{-+}, 0, \tau_{he}^{--}, 0, 0, \tau_{hh}^{--})^T. \quad (\text{A16})$$

Each scattering problem of the form of Eq. (12) is therefore an  $8 \times 8$  linear eigenvalue problem. The complexity of the propagators  $U_l(x, x')$ , though, requires a numerical treatment of the problem.

## APPENDIX B: GREEN’S FUNCTION FOR SEMI-INFINITE SECTION

The retarded Green’s function in a semi-infinite section, attached to a scattering region, can be calculated using *outgoing wave boundary conditions*. Now we construct the retarded Green’s function in the left lead of our system, i.e., for  $x, x' < 0$ . Therefore, we separate the Green’s function into

$$\hat{G}^R(x, x', \omega) = \hat{G}_{<}^R(x, x', \omega)\theta(x' - x) + \hat{G}_{>}^R(x, x', \omega)\theta(x - x'), \quad (\text{B1})$$

and choose

$$\hat{G}_{<}^R(x, x', \omega) = \Phi_{\text{in},1}(x)A_1^T(x') + \Phi_{\text{in},2}(x)A_2^T(x') + \Phi_{\text{in},3}(x)A_3^T(x') + \Phi_{\text{in},4}(x)A_4^T(x'), \quad (\text{B2})$$

$$\hat{G}_{>}^R(x, x', \omega) = \Phi_{\text{in},5}(x)A_5^T(x') + \Phi_{\text{in},6}(x)A_6^T(x') + \Phi_{\text{in},7}(x)A_7^T(x') + \Phi_{\text{in},8}(x)A_8^T(x') \quad (\text{B3})$$

with the unknown vectors  $A_j(x')^T = (A_{j1}, A_{j2}, A_{j3}, A_{j4})^T$ . Furthermore, the eigenstates  $\Phi_{\text{in},j}(x)$  are given by

$$\Phi_{\text{in},j}(x) = U_0(x, 0)\Phi_{\text{in},j}(0). \quad (\text{B4})$$

Inserting Eqs. (B2) and (B3) in Eq. (15) yields the solution for the vectors  $A_j(x')$  and thus the form of the retarded Green's function in the TI leftmost of the scattering region for  $x, x' < 0$ . Adopting the notation of Eq. (17), we obtain

$$\hat{G}_{++}^R(x, x', \omega) = -i \begin{pmatrix} e^{i(x-x')(\mu+\omega)\theta(x-x')} & 0 & 0 & 0 \\ e^{-i(x+x')(\mu+\omega)r_{ee}^{++}} & e^{-i(x-x')(\mu+\omega)\theta(x'-x)} & 0 & e^{i[x'(\mu-\omega)-x(\mu+\omega)]r_{he}^{++}} \\ e^{i[x(\mu-\omega)-x'(\mu+\omega)]r_{eh}^{++}} & 0 & e^{i(x-x')(\mu-\omega)\theta(x'-x)} & e^{i(x+x')(\mu-\omega)r_{hh}^{++}} \\ 0 & 0 & 0 & e^{-i(x-x')(\mu-\omega)\theta(x-x')} \end{pmatrix}, \quad (\text{B5})$$

$$\hat{G}_{--}^R(x, x', \omega) = -i \begin{pmatrix} e^{-i(x-x')(\mu+\omega)\theta(x'-x)} & e^{-i(x+x')(\mu+\omega)r_{ee}^{--}} & e^{i[x'(\mu-\omega)-x(\mu+\omega)]r_{he}^{--}} & 0 \\ 0 & e^{i(x-x')(\mu+\omega)\theta(x-x')} & 0 & 0 \\ 0 & 0 & e^{-i(x-x')(\mu-\omega)\theta(x-x')} & 0 \\ 0 & e^{i[x(\mu-\omega)-x'(\mu+\omega)]r_{eh}^{--}} & e^{i(x+x')(\mu-\omega)r_{hh}^{--}} & e^{i(x-x')(\mu-\omega)\theta(x'-x)} \end{pmatrix}, \quad (\text{B6})$$

$$\hat{G}_{-+}^R(x, x', \omega) = -i \begin{pmatrix} 0 & 0 & 0 & 0 \\ 0 & e^{-i(x+x')(\mu+\omega)r_{ee}^{+-}} & e^{i[x'(\mu-\omega)-x(\mu+\omega)]r_{he}^{+-}} & 0 \\ 0 & e^{i[x(\mu-\omega)-x'(\mu+\omega)]r_{eh}^{+-}} & e^{i(x+x')(\mu-\omega)r_{hh}^{+-}} & 0 \\ 0 & 0 & 0 & 0 \end{pmatrix}, \quad (\text{B7})$$

and

$$\hat{G}_{+-}^R(x, x', \omega) = -i \begin{pmatrix} e^{-i(x+x')(\mu+\omega)r_{ee}^{+-}} & 0 & 0 & e^{i[x'(\mu-\omega)-x(\mu+\omega)]r_{he}^{+-}} \\ 0 & 0 & 0 & 0 \\ 0 & 0 & 0 & 0 \\ e^{i[x(\mu-\omega)-x'(\mu+\omega)]r_{eh}^{+-}} & 0 & 0 & e^{i(x+x')(\mu-\omega)r_{hh}^{+-}} \end{pmatrix}. \quad (\text{B8})$$

Eqs. (B5)–(B8) define the lead Green's function that is used in the main text to construct the Green's function anywhere in the heterojunction.

- 
- [1] C. L. Kane and E. J. Mele, *Phys. Rev. Lett.* **95**, 226801 (2005).  
[2] C. L. Kane and E. J. Mele, *Phys. Rev. Lett.* **95**, 146802 (2005).  
[3] B. A. Bernevig, T. A. Hughes, and S.-C. Zhang, *Science* **314**, 1757 (2006).  
[4] M. König, S. Wiedmann, C. Brüne, A. Roth, H. Buhmann, L. W. Molenkamp, X.-L. Qi, and S.-C. Zhang, *Science* **318**, 766 (2007).  
[5] A. Roth, C. Brüne, H. Buhmann, L. W. Molenkamp, J. Maciejko, X. Qi, and S. Zhang, *Science* **325**, 294 (2009).  
[6] C. Liu, T. L. Hughes, X.-L. Qi, K. Wang, and S.-C. Zhang, *Phys. Rev. Lett.* **100**, 236601 (2008).  
[7] I. Knez, R.-R. Du, and G. Sullivan, *Phys. Rev. Lett.* **107**, 136603 (2011).  
[8] I. Knez, R.-R. Du, and G. Sullivan, *Phys. Rev. Lett.* **109**, 186603 (2012).  
[9] L. Du, I. Knez, G. Sullivan, and R.-R. Du, *Phys. Rev. Lett.* **114**, 096802 (2015).  
[10] V. S. Pribiag, A. J. A. Beukman, F. Qu, M. C. Cassidy, C. Charpentier, W. Wegscheider, and L. P. Kouwenhoven, *Nat. Nanotechnol.* **10**, 593 (2015).  
[11] C. Wu, B. A. Bernevig, and S.-C. Zhang, *Phys. Rev. Lett.* **96**, 106401 (2006).  
[12] F. Geissler, F. Crépin, and B. Trauzettel, *Phys. Rev. B* **89**, 235136 (2014).  
[13] N. T. Ziani, F. Crépin, and B. Trauzettel, *Phys. Rev. Lett.* **115**, 206402 (2015).  
[14] N. Traverso Ziani, C. Fleckenstein, G. Dolcetto, and B. Trauzettel, *Phys. Rev. B* **95**, 205418 (2017).  
[15] L. Fu and C. L. Kane, *Phys. Rev. Lett.* **100**, 096407 (2008).  
[16] L. Fu and C. L. Kane, *Phys. Rev. B* **79**, 161408 (2009).  
[17] S. Hart, H. Ren, T. Wagner, P. Leubner, M. Mühlbauer, C. Brüne, H. Buhmann, L. W. Molenkamp, and A. Yacoby, *Nat. Phys.* **10**, 638 (2014).  
[18] V. L. Berezinskii, *JETP Lett.* **20**, 287 (1974).  
[19] Y. Tanaka and A. A. Golubov, *Phys. Rev. Lett.* **98**, 037003 (2007).  
[20] Y. Tanaka, M. Sato, and N. Nagaosa, *J. Phys. Soc. Jpn.* **81**, 011013 (2012).  
[21] Y. Tanaka, A. A. Golubov, S. Kashiwaya, and M. Ueda, *Phys. Rev. Lett.* **99**, 037005 (2007).  
[22] M. Eschrig, T. Löfwander, T. Champel, J. C. Cuevas, J. Kopu, and G. Schön, *J. Low Temp. Phys.* **147**, 457 (2007).  
[23] Y. Tanaka, Y. Tanuma, and A. A. Golubov, *Phys. Rev. B* **76**, 054522 (2007).

- [24] J. Linder and A. V. Balatsky, [arXiv:1709.03986](#).
- [25] J. Cayao and A. M. Black-Schaffer, *Phys. Rev. B* **96**, 155426 (2017).
- [26] A. M. Black-Schaffer and A. V. Balatsky, *Phys. Rev. B* **86**, 144506 (2012).
- [27] Y. Asano and Y. Tanaka, *Phys. Rev. B* **87**, 104513 (2013).
- [28] F. Crépin, P. Bursset, and B. Trauzettel, *Phys. Rev. B* **92**, 100507(R) (2015).
- [29] F. Keidel, P. Bursset, and B. Trauzettel, *Phys. Rev. B* **97**, 075408 (2018).
- [30] F. S. Bergeret, A. F. Volkov, and K. B. Efetov, *Rev. Mod. Phys.* **77**, 1321 (2005).
- [31] M. Alidoust and J. Linder, *Phys. Rev. B* **82**, 224504 (2010).
- [32] T. S. Khaire, M. A. Khasawneh, W. P. Pratt, and N. O. Birge, *Phys. Rev. Lett.* **104**, 137002 (2010).
- [33] Y. Asano, A. A. Golubov, Y. V. Fominov, and Y. Tanaka, *Phys. Rev. Lett.* **107**, 087001 (2011).
- [34] M. Alidoust, K. Halterman, and J. Linder, *Phys. Rev. B* **89**, 054508 (2014).
- [35] A. Di Bernardo, Z. Salman, X. L. Wang, M. Amado, M. Egilmez, M. G. Flokstra, A. Suter, S. L. Lee, J. H. Zhao, T. Prokscha, E. Morenzoni, M. G. Blamire, J. Linder, and J. W. A. Robinson, *Phys. Rev. X* **5**, 041021 (2015).
- [36] R. Beiranvand, H. Hamzehpour, and M. Alidoust, *Phys. Rev. B* **96**, 161403(R) (2017).
- [37] D. Beckmann, H. B. Weber, and H. v. Löhneysen, *Phys. Rev. Lett.* **93**, 197003 (2004).
- [38] S. Russo, M. Kroug, T. M. Klapwijk, and A. F. Morpurgo, *Phys. Rev. Lett.* **95**, 027002 (2005).
- [39] J. P. Morten, A. Brataas, and W. Belzig, *Phys. Rev. B* **74**, 214510 (2006).
- [40] J. Cayssol, *Phys. Rev. Lett.* **100**, 147001 (2008).
- [41] P. Bursset, B. Lu, H. Ebisu, Y. Asano, and Y. Tanaka, *Phys. Rev. B* **93**, 201402(R) (2016).
- [42] C. Benjamin, *Phys. Rev. B* **74**, 180503 (2006).
- [43] B. H. Wu, W. Yi, J. C. Cao, and G.-C. Guo, *Phys. Rev. B* **90**, 205435 (2014).
- [44] X.-L. Qi, T. L. Hughes, and S.-C. Zhang, *Nat. Phys.* **4**, 273 (2008).
- [45] J. I. Väyrynen and T. Ojanen, *Phys. Rev. Lett.* **107**, 166804 (2011).
- [46] C. P. Orth, R. P. Tiwari, T. Meng, and T. L. Schmidt, *Phys. Rev. B* **91**, 081406(R) (2015).
- [47] C. Fleckenstein, N. Traverso Ziani, and B. Trauzettel, *Phys. Rev. B* **94**, 241406(R) (2016).
- [48] S. Porta, F. M. Gambetta, N. Traverso Ziani, D. M. Kennes, M. Sassetti, and F. Cavaliere, *Phys. Rev. B* **97**, 035433 (2018).
- [49] J. Li, W. Pan, B. A. Bernevig, and R. M. Lutchyn, *Phys. Rev. Lett.* **117**, 046804 (2016).
- [50] J. C. Y. Teo and C. L. Kane, *Phys. Rev. B* **79**, 235321 (2009).
- [51] C.-X. Liu, J. C. Budich, P. Recher, and B. Trauzettel, *Phys. Rev. B* **83**, 035407 (2011).
- [52] F. Dolcini, *Phys. Rev. B* **83**, 165304 (2011).
- [53] G. Dolcetto, S. Barbarino, D. Ferraro, N. Magnoli, and M. Sassetti, *Phys. Rev. B* **85**, 195138 (2012).
- [54] T. L. Schmidt, S. Rachel, F. von Oppen, and L. I. Glazman, *Phys. Rev. Lett.* **108**, 156402 (2012).
- [55] J. I. Väyrynen, M. Goldstein, and L. I. Glazman, *Phys. Rev. Lett.* **110**, 216402 (2013).
- [56] N. Kainaris, I. V. Gornyi, S. T. Carr, and A. D. Mirlin, *Phys. Rev. B* **90**, 075118 (2014).
- [57] L. Vannucci, F. Ronetti, G. Dolcetto, M. Carrega, and M. Sassetti, *Phys. Rev. B* **92**, 075446 (2015).
- [58] F. Ronetti, L. Vannucci, G. Dolcetto, M. Carrega, and M. Sassetti, *Phys. Rev. B* **93**, 165414 (2016).
- [59] C. Timm, *Phys. Rev. B* **86**, 155456 (2012).
- [60] A. R. Akhmerov, J. P. Dahlhaus, F. Hassler, M. Wimmer, and C. W. J. Beenakker, *Phys. Rev. Lett.* **106**, 057001 (2011).
- [61] W. L. McMillan, *Phys. Rev.* **175**, 559 (1968).
- [62] B. Lu and Y. Tanaka, [arXiv:1512.00916](#).
- [63] S. Kashiwaya and Y. Tanaka, *Rep. Prog. Phys.* **63**, 1641 (2000).
- [64] W. J. Herrera, P. Bursset, and A. L. Yeyati, *J. Phys.: Condens. Matter* **22**, 275304 (2010).
- [65] H. Ebisu, B. Lu, J. Klinovaja, and Y. Tanaka, *Prog. Theor. Exp. Phys.* **2016**, 083101 (2016).
- [66] P. Adroguer, C. Grenier, D. Carpentier, J. Cayssol, P. Degiovanni, and E. Orignac, *Phys. Rev. B* **82**, 081303(R) (2010).
- [67] N. M. Chtchelkatchev, *JETP Lett.* **78**, 230 (2003).